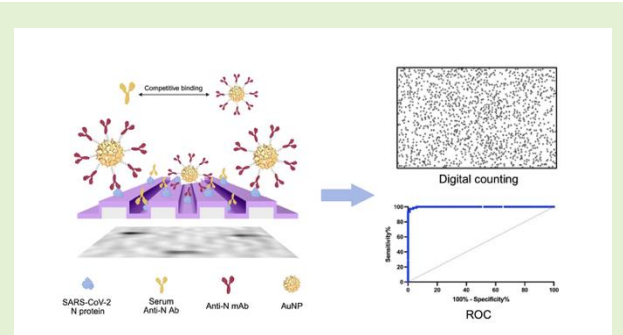


# Digital Immunoassay for Rapid Detection of SARS-CoV-2 exposure in a Broad Spectrum of Animals

Siyan Li<sup>1a</sup>, Weijing Wang<sup>2,3a</sup>, Weinan Liu<sup>3,4</sup>, Chi Chen<sup>1</sup>, Skye Shepherd<sup>2,3</sup>, Fangfeng Yuan<sup>1b</sup>, Jennifer M. Reinhart<sup>5</sup>, Diego G. Diel<sup>6</sup>, Brian T. Cunningham<sup>2,3,4,7,8\*</sup>, Ying Fang<sup>1,7\*</sup>

**Abstract**—The ability of Severe Acute Respiratory Syndrome Coronavirus 2 (SARS-CoV-2) to infect a wide-range of species raises significant concerns regarding both human-to-animal and animal-to-human transmission. There is an increasing demand for highly sensitive, rapid, and simple diagnostic assays capable of detecting viral infection across various species. In this study, we developed a biosensor assay based on a blocking ELISA (bELISA) immunoassay format. The assay employs a photonic crystal (PC) biosensor, gold-nanoparticle (AuNP) tags, SARS-CoV-2 nucleocapsid (N) protein, and specific anti-N monoclonal antibody (mAb) to detect antibody responses in animals exposed to SARS-CoV-2. Based on an evaluation of 162 cat serum samples with known antibody status, an optimal percentage of inhibition (PI) cut-off value of 0.5877 resulted in a diagnostic sensitivity of 97.80% and a diagnostic specificity of 98.67%. The assay demonstrated high repeatability with low variation coefficients across different conditions, ensuring consistent performance. Additionally, the assay successfully detected anti-N antibody responses in ferrets and deer as early as 14 days post-infection (DPI), and in cats infected with both Omicron (B.1.1.529) and B.1 D614G (B.1) variants as early as 7 DPI. These results highlight the assay's ability to detect infections early and reliably across species and its capability to identify multiple variants of SARS-CoV-2. This test platform provides an important tool for rapid field surveillance of SARS-CoV-2 infection across multiple species.

**Index Terms**—SARS-CoV-2 detection, photonic crystal biosensor, gold nanoparticles, monoclonal antibody, blocking biosensor assay.



## I. INTRODUCTION

The global outbreak of Coronavirus Disease 2019 (COVID-19) has been primarily driven by the rapid

and widespread transmission of Severe Acute Respiratory Syndrome Coronavirus 2 (SARS-CoV-2) [1]. The virus has the ability to infect a broad array of

<sup>1</sup>Department of Pathobiology, University of Illinois at Urbana-Champaign, Urbana, IL, USA;

<sup>2</sup>Department of Bioengineering, University of Illinois at Urbana-Champaign, Urbana, IL, USA;

<sup>3</sup>Nick Holonyak Micro and Nanotechnology Laboratory, University of Illinois Urbana-Champaign, IL 61802 USA

<sup>4</sup>Department of Electrical and Computer Engineering, University of Illinois at Urbana-Champaign, Urbana, IL, USA;

<sup>5</sup>Department of Veterinary Clinical Medicine, University of Illinois at Urbana-Champaign, Urbana, IL, USA;

<sup>6</sup>Department of Population Medicine and Diagnostic Sciences, Cornell University, Ithaca, New York, USA;

<sup>7</sup>Carl R. Woese Institute for Genomic Biology, University of Illinois at Urbana-Champaign, Urbana, IL, USA.

<sup>8</sup>Cancer center at Illinois, University of Illinois Urbana-Champaign, IL 61802 USA

<sup>a</sup>Siyan Li and Weijing Wang contribute equally to this work.

<sup>b</sup>Current address: Massachusetts Institute of Technology, Cambridge, MA 02139

\*Corresponding authors: Brian T. Cunningham, Ying Fang.

Siyan Li is affiliated with Department of Pathobiology, University of Illinois Urbana-Champaign, IL 61802 USA (e-mail: sl165@illinois.edu).

Weijing Wang is affiliated with Department of Bioengineering, Nick Holonyak Micro and Nanotechnology Laboratory, University of Illinois Urbana-Champaign, IL 61802 USA (e-mail: weijing4@illinois.edu).

Weinan Liu is affiliated with Department of Electrical and Computer Engineering, Nick Holonyak Micro and Nanotechnology Laboratory, University of Illinois Urbana-Champaign, IL 61802 USA (e-mail: weinanl3@illinois.edu).

species, leading to significant concerns regarding cross-species transmission, including human-to-animal and animal-to-human transmission [1, 2]. The situation is further complicated by the rapid mutations of viral RNA genome, which occur as it crosses between different hosts, potentially leading to emergence of new strains that could undermine the current control and prevention measures [3].

One of the key strategies for disease control and prevention is the early and rapid identification of infected individuals and animals, which requires highly sensitive and rapid diagnostic assays. For SARS-CoV-2, the assays must be capable of detecting the virus across a variety of species in order to facilitate timely isolation of affected individuals/animals to prevent further spread of the virus. Laboratory diagnostic tests for SARS-CoV-2 fall into four main categories: virus isolation [4], viral antigen detection [5, 6], molecular (viral nucleic acid) diagnostics [7], and host antibody detection [8], with each serving a unique purpose in identifying the virus infection. Serological assays, especially enzyme linked immunosorbent assay (ELISA), are commonly utilized to detect specific host antibodies against SARS-CoV-2, providing insights into past virus exposure [9]. While indirect ELISA is highly sensitive and specific, its dependency on species-specific secondary antibodies limits its ability to detect antibodies across a diverse range of hosts [9]. Blocking ELISA (bELISA) stands out for its increased specificity in detecting antibody responses from a broad spectrum of host species [10]. The bELISA incorporates a monoclonal antibody (mAb) that targets a conserved epitope in a viral antigen. The test readout is based on the mAb binding ability; thus, a species-specific secondary antibody is not required. Such a test platform will allow the assay to be applicable to all animal species and humans.

While bELISA offers increased specificity for detecting antibodies across a broad range of species, it still requires laboratory settings and complex workflows, limiting its application for rapid field use. Recently, there has been a rapid progress in the development of

nanotechnology-based biosensors, which aim to overcome these limitations by offering more portable, cost-effective, and rapid alternatives. Nanotechnology-based biosensors have shown growing promise in SARS-CoV-2 serological diagnostics, particularly for use beyond clinical labs. They offer advantages such as speed, portability, and ease of use, making them well-suited for field deployment [11]. For instance, the ePAD platform detects SARS-CoV-2 antibodies in animal serum via electrical signals [12], while luminescent biosensors use split luciferase fragments to signal antibody binding without requiring antigen immobilization [13]. However, most systems are optimized for human antibodies and may lack cross-species compatibility. A MetaSPR-based optical biosensor enables high-throughput, multispecies antibody detection but can be affected by background noise due to non-specific binding [14]. Therefore, continued development is needed to achieve biosensors that combine cross-species compatibility with accurate and rapid serological performance.

In this work, we employed a novel form of biosensor, where a Photonic Crystal (PC) is integrated with a portable and inexpensive detection instrument for quantitative detection of gold nanoparticle (AuNP) tags. In this “blocking biosensor assay”, each AuNP represents one antigen-antibody binding interaction that can be digitally counted. The assay is an alternative to bELISA that does not require enzymatic amplification, thus providing an immediate readout without the need for enzyme-substrate interactions to generate colored or fluorescent products.

A PC is a sub-wavelength grating structure consisting of a periodic arrangement of a low refractive index material coated with a high refractive index layer. At a particular resonant wavelength, complete interference occurs, and no light is transmitted, resulting in nearly 100% reflection efficiency [15-19]. The resonant reflectance magnitude is modulated by the addition of a light-absorbing AuNP upon the PC surface, resulting in a large reduction in the reflected intensity. By measuring

---

Skye Shepherd, is affiliated with Department of Bioengineering, Nick Holonyak Micro and Nanotechnology Laboratory, University of Illinois Urbana-Champaign, IL 61802 USA (e-mail: skyes2@illinois.edu)

Chi Chen is affiliated with Department of Pathobiology, University of Illinois Urbana-Champaign, IL 61802 USA (e-mail: chenchi2@illinois.edu).

Fangfeng Yuan is affiliated with Department of Pathobiology, University of Illinois Urbana-Champaign, IL 61802 USA, currently affiliated with Massachusetts Institute of Technology, Cambridge, MA 02139, USA. (e-mail: fy9@mit.edu).

Jennifer M. Reinhart is affiliated with Department of Veterinary Clinical Medicine, University of Illinois at Urbana-Champaign, Urbana, IL, 61802, USA (e-mail: jreinha2@illinois.edu).

Diego G. Diel is affiliated with Department of Population Medicine and Diagnostic Sciences, Cornell University, Ithaca, New York, 14850, USA (e-mail: dgdiel@cornell.edu).

Brian T. Cunningham is affiliated with Department of Bioengineering, Department of Electrical and Computer Engineering, Nick Holonyak Micro and Nanotechnology Laboratory, Carl R. Woese Institute for Genomic Biology, Cancer Center at Illinois, University of Illinois Urbana-Champaign, IL 61802 USA (e-mail: bcunning@illinois.edu)

Ying Fang is affiliated with Department of Pathobiology, Carl R. Woese Institute for Genomic Biology, University of Illinois Urbana-Champaign, IL 61802 USA (e-mail: yingf@illinois.edu).

the reflected intensity from a red LED on a pixel-by-pixel basis across the PC, images of attached AuNPs may be gathered by illuminating the structure with collimated light through the transparent substrate, while the top surface of the PC is immersed in aqueous solution [20]. Recently, our group developed a technique called Photonic Resonator Absorption Microscopy (PRAM) that can visualize individual AuNP tags on a PC surface through resonance coupling [8, 21-26]. By immobilizing target-activated AuNP probes on a PC surface, PRAM has been used to quantify nucleic acids and proteins with single-particle resolution [8, 21, 22, 25-29]. This capability has enabled highly sensitive detection across various targets: PRAM detected small RNAs down to 0.25 fM in 30 minutes and microRNA as low as 100 aM within 2 hours [21]. It also achieved single-particle resolution in SARS-CoV-2 antibody detection, with a 15-minute, wash-free assay reaching a LOD of  $26.7 \pm 7.7$  pg/mL [8]. These assays exhibited a dynamic range of five orders of magnitude using only  $\sim 10$   $\mu$ L of sample. We recently designed a portable version of the PRAM instrument with a cost of components totaling \$7,000 and current research efforts are directed towards a miniaturized PRAM instrument with a cost of \$500 [30].

In this study, we integrated the bELISA immunoassay format with the PRAM detection system to create a novel blocking biosensor assay, which combines the advantages of both methodologies to generate a new serological detection platform. This novel approach presents an advanced tool for the quick identification of SARS-CoV-2 exposure. This advancement not only enhances our diagnostic capabilities but also significantly contributes to our collective efforts in understanding and controlling the cross-species transmission of SARS-CoV-2 infection.

## II. MATERIALS AND METHODS

### A. Preparation of antigen and monoclonal antibody

The nucleocapsid (N) protein of SARS-CoV-2 was expressed in *E. coli* as a 6x His-tagged recombinant protein. The N antigen was produced and purified using the methods described in our previous study [31]. Purified protein was dialyzed using 1x phosphate-buffered saline (PBS) solution under 4°C and then concentrated by polyethylene glycol 8000 (Thermo Fisher Scientific, 320 Waltham, MA). The SARS-CoV-2 specific anti-N mAb #127-3 was generated in our previous study [31].

### B. Synthesis of Spiky AuNPs

The spiky AuNPs were synthesized using a two-step growth method. Initially, 5 mL of a commercially obtained 20-nm spherical AuNP seed solution (Cytodiagnosics, 0.05 mg/mL) was incubated in 3 mL of 2 mM sodium citrate solution for 30 minutes with

moderate shaking. After incubation, the nanoparticles were washed three times by centrifugation at 20,000  $\times g$  once and then redispersed in 2 mL of a 3 mM sodium citrate solution (Sigma-Aldrich). Next, 4 mL of a 0.5 mM HAuCl solution (Sigma-Aldrich) was heated to 300 °C, and 2 mL of the nanoparticle seed solution was rapidly injected into the solution while stirring vigorously at 700 rpm. The mixture was allowed to react for 10 minutes at 260 °C, during which the solution color changed from brown to burgundy. The solution was then cooled under stirring for another 10 minutes, followed by washing with 2 mM sodium citrate and centrifugation at 4,000  $\times g$  for 10 minutes, repeated three times. The resulting smooth spherical core-shell AuNPs were resuspended in 1.5 mL of a 2 mM sodium citrate solution to serve as the seeds for the next step. For the growth of the spiky gold coating, a mixture of 5 mL of 0.25 mM HAuCl, NP seeds (Absorbance at 535 nm = 0.3, 65  $\mu$ L) was stirred vigorously. Then, 11  $\mu$ L of 1% (w/v) sodium citrate was added, followed by the quick injection of 500  $\mu$ L of a 30 mM hydroquinone solution (Sigma-Aldrich) to initiate the reaction. The growth solution was allowed to react for 30 minutes at room temperature under constant stirring (700 rpm), during which the solution gradually changed from burgundy to blue. For long-term storage, 50  $\mu$ L of a 1% (w/v) Pluronic F-127 solution was incorporated into the AuNPs. Right before use, the spiky AuNPs were subjected to three washes at 800  $\times g$  for 7 minutes, followed by resuspended in a 0.1% (w/v) Pluronic F-127 solution.

### C. Anti-N mAb-AuNP conjugation

Initially, a fresh aliquot of SH-PEG-NHS (MW 5000, JenKem Technology, Plano, TX, USA) was diluted in Milli-Q water to a final concentration of 4  $\mu$ M. Subsequently, 20  $\mu$ g of the anti-SARS-CoV-2 N mAb was gently mixed with the SH-PEG-NHS solution at a 1:1.5 molar ratio in PBS buffer at room temperature. This mixture was then incubated on a shaker at 900 rpm for 2 hours to allow the NHS ester group on the PEG to react with the amine group on the mAb, facilitating the conjugation. After conjugation, the mixture was filtered through a 50 K centrifuge filter (Millipore Sigma™ Amicon™ Ultra-0.5 Centrifugal Filter Units) to remove any unbound PEG, with the antibody washed three times at 14000  $\times g$  for 10 minutes in PBS. The SH-PEG-mAb was collected by inverting and centrifuging at 1000  $\times g$  for 2 minutes. All centrifugation steps were performed at 4°C. The concentrated SH-PEG-mAb conjugate was then quickly combined with AuNPs in a non-stick microcentrifuge tube. The mixture is incubated overnight at 4°C on a shaker, allowing the mAb to efficiently bind to the AuNPs. Post-incubation, the conjugates undergo Dynamic Light Scattering (DLS) analysis to verify the increase in particle size, indicating successful conjugation. The solution was then blocked by

adding filtered 2% bovine serum albumin (BSA) in PBS to prevent nonspecific interactions. Excess mAbs were removed by centrifugation ( $1000 \times g$ , 5 min), and the conjugates were resuspended in a  $0.1 \times$  PBST (Pierce™) solution for final storage at  $4^{\circ}\text{C}$ , where they remained stable for up to one week. This preparation was critical for subsequent applications in the blocking biosensor assays, as the functionality and stability of the conjugates directly impact the assay's performance. To assess the conjugation performance, DLS measurements showed that mAb-AuNPs displayed a distinct increase of  $\sim 22$  nm in average diameter compared to non-functionalized bare AuNPs (132 nm vs 110 nm). In addition, UV-visible spectroscopy revealed a red shift in the peak absorbance wavelength, increasing by  $\sim 10$  nm from 615 nm to 625 nm following conjugation, further supporting effective surface modification of the nanoparticles.

#### D. PC biosensor preparation and functionalization

The PC biosensors were fabricated on 8-inch diameter glass substrates (Moxtek, Orem, UT), which were then cut into  $10 \times 12$  mm<sup>2</sup> pieces for experimental use. The PCs feature a periodic grating structure with a period of 380 nm and a depth of 97 nm, created through reactive ion etching on the glass. Over this grating, a 98.5 nm thick TiO<sub>2</sub> layer, with a refractive index of 2.25 was deposited. This configuration allows for the efficient resonant reflection at a wavelength of 625 nm when the PC surface was submerged in aqueous solution. PCs were single-use only and discarded after each assay.

The PC was attached to a coverslip using UV glue (Norland Optical Adhesive NOA 68) and cured with UV light for two minutes. Next, the PC underwent a cleaning process to remove contaminants. The PC was first immersed in acetone in a glass jar and sonicated for two minutes. This process was repeated with isopropyl alcohol (IPA) and Milli-Q water to ensure thorough cleansing. The PC was then dried with nitrogen and placed in a  $60^{\circ}\text{C}$  oven for 10 minutes to eliminate residual moisture. Following cleaning, the PC was treated using an oxygen plasma generator, to activate the surface for further processing. A 5% solution of 3-aminopropyltriethoxysilane (APTES, Sigma-Aldrich) in tetrahydrofuran (THF, Sigma-Aldrich) was prepared by mixing 2.5 mL of APTES with 47.5 mL of THF. The activated PC was transferred into this APTES solution, where it was incubated for one hour on a shaker at room temperature. Following incubation, the APTES solution was discarded, and the PC was further cleaned using THF, acetone, ethanol, and Milli-Q water in a sonication for two minutes. Finally, the PC was dried, wrapped in aluminum foil to protect it from light, and stored in a desiccator for up to one month, ensuring its readiness for subsequent functionalization and assays.

#### E. Sample sources

The control serum standards utilized for assay development were prepared from samples obtained in our previous cat experiment [32]. The positive control standard was created using serum samples from experimental cats that were infected with SARS-CoV-2 variants D614G (B.1), Delta (B.1.617.2), and Omicron (B.1.1.529) at 14 days post-infection (DPI). Similarly, the negative control standard was made from serum samples of negative control cats. Large volumes of positive sera from different cats were pooled to create a single lot of positive control standard, while large volumes of negative sera were pooled to generate a single lot of negative control standard.

To validate the biosensor assay, a total of 162 serum samples from cats were obtained from the Clinical Pathology Laboratory of the University of Illinois Veterinary Diagnostic Laboratory in Urbana, IL. These samples were originally submitted for unrelated clinical purposes during 2022 to 2024. We used excess serum after clinical evaluations. Following serological test with multiple assays, 86 samples were confirmed positive for SARS-CoV-2 specific antibodies, while 76 samples tested negative [33]. Since the serum was not collected specifically for this study, the sample collection did not qualify as animal use under regulations, and therefore did not require approval from the University of Illinois Institutional Animal Care and Use Committee [33]. To maintain confidentiality, all identifiable information, such as animal names and addresses, was removed from the data, and the new project-specific identifiers were assigned to each sample.

For validation of the biosensor assay across multiple animal species, two sets of animal serum samples with known infection status were used. The first set contained 5 positive and 3 negative serum samples collected from ferrets infected by SARS-CoV-2 isolate NYI67-20 (B.1 lineage) [32]. The second set contained 5 positive and 3 negative serum samples collected from the deer infected with the same SARS-CoV-2 isolate NYI67-20 (B.1 lineage). To determine the seroconversion using the blocking biosensor assay, a panel of serum samples was collected from 3 experimental cats in a time course study at 0, 3, 5, 7, and 14 days post-inoculation. Among these 3 cats, one was infected with SARS-CoV-2 Omicron variant, another one was infected with D614G variant, and one negative control cat was included for comparison.

#### F. Procedure for blocking biosensor assay

One day before the assay, the APTES-functionalized PC was removed from the desiccator. Polydimethylsiloxane (PDMS) gasket was then cut to match the size of the PC, with six circular holes (3 mm diameter) created in each gasket using a biopsy punch to hold the reaction mixtures. The PDMS gasket was

securely attached to the PC surface by pressing them firmly. To prepare the DSC solution, 5 mg of DSC (Sigma-Aldrich) was dissolved in 100  $\mu\text{L}$  of DMSO and then diluted with 900  $\mu\text{L}$  of water to a final volume of 1 mL. Each reaction well was then filled with the DSC solution and incubated for 20 minutes. After incubation, the DSC solution was removed, and 10  $\mu\text{L}$  of 0.08 mg/mL recombinant SARS-CoV-2 N protein was added to each well, followed by overnight incubation at 4°C. Subsequently, each well was treated with 20  $\mu\text{L}$  of 1  $\times$  Power Block (Thermo Fisher) and incubated at 37°C for 1 hour to minimize nonspecific binding of AuNPs during the assay. The PC was then washed three times with 1  $\times$  PBST. Finally, serum samples, diluted 4 times with blocking buffer, were added to the PC surface and incubated at 37°C for 1 hour on a shaker to facilitate thorough binding.

For the assay setup, the PC was placed under the PRAM instrument, and a background image was captured. Serum samples were then removed from the wells by pipetting, and 20  $\mu\text{L}$  of AuNPs-PEG-mAb conjugates (Abs =  $1.20 \pm 0.05$ , diluted with 0.1  $\times$  PBS) were added to the PDMS well. The reaction was allowed to proceed for 15 minutes. Afterward, the PC was aligned under the PRAM to capture the reaction image. This process was repeated for each concentration, with each sample tested in duplicate to ensure repeatability. Image analysis was performed using a custom Matlab algorithm [34], which adjusts the threshold and other parameters to accurately count the particles while minimizing background interference. This detailed approach enabled precise quantification of SARS-CoV-2 anti-N mAbs effectively.

### III. RESULTS

#### A. Design of blocking biosensor digital immunoassay

The blocking biosensor assay adopts the same immunological structure as the bELISA but integrates PC and AuNP tags for signal quantification. Figure 1 illustrates the design of blocking biosensor immunoassay for the detection of SARS-CoV-2 N protein specific antibodies in serum samples. To begin, anti-N mAb-AuNPs were prepared by conjugating anti-N mAb #127-3 with 110 nm diameter AuNPs via heterobifunctional SH-PEG-NHS linkers. The NHS ester enabled covalent bonding to the mAb's amine groups, while the thiol end bound the complex to the AuNP surface, forming a stable conjugate suitable for downstream biosensing (Figure 1A). PC was functionalized with APTES and DSC to enable covalent immobilization. N proteins were loaded into PDMS wells attached to the PC surface and incubated overnight (Figure 1B). To minimize

nonspecific binding, unreacted sites on both the AuNPs and PC surface were blocked with BSA. Animal serum samples for testing were then added to the PDMS well and incubated for 1 hour at 37°C. After removing the serum samples, the mAb-AuNPs were introduced into the PDMS wells. As shown in Figure 1C, in this 2-step assay, virus specific antibodies in serum (yellow) quickly occupy the binding sites on the viral N protein, preventing mAb-AuNPs from binding to the viral protein on the PC surface. In contrast, negative serum (lacking virus specific antibodies) allows the mAb to bind to the viral protein, forming a AuNPs-mAb-N protein immunocomplex particle captured onto the PC surface. The captured AuNPs locally quench the PC reflection efficiency. Peak intensity value images are obtained by PRAM, enabling the digital counting of particles for quantitative analysis within 15 minutes. The reduction in anti-N mAb-AuNPs binding to the N protein on the PC surface is directly proportional to the quantity of anti-N antibodies in the serum sample, providing an accurate quantitative measurement of serum antibody levels.

#### B. Determination of diagnostic sensitivity and specificity

To evaluate the performance of the blocking biosensor assay for antibody detection, we tested a cohort of cat serum samples with known antibody status, which includes 86 known positive and 76 known negative samples from clinical infected cats. These samples had confirmed antibody status from our previous studies [32, 33]. To normalize the results, AuNP count per field of view (FOV) were converted into a percentage inhibition (PI) value, calculated as follows:  $PI = [1 - (\text{Test Value} / \text{Negative Control Value})]$ . A higher PI value indicates a greater degree of inhibition, and reflects a higher concentration of anti-N antibodies present in the sample. As shown in Figure 2A, the positive samples exhibited significantly higher PI values compared to the negative samples, demonstrating clear separation between the two groups. Based on the distribution of PI values, a cut-off value of 0.5877 was selected by plotting all PI values in GraphPad Prism and choosing the point that provided the highest combined diagnostic sensitivity and specificity. At this threshold, the assay achieved a diagnostic sensitivity of 97.80% and specificity of 98.67%. To further assess the overall diagnostic performance, a receiver operating characteristic (ROC) curve was generated (Figure 2B). The area under curve (AUC) yield from the ROC analysis indicates overall test accuracy, where an AUC of 1 represents perfect diagnostic accuracy and AUC above 0.9 is generally considered highly accurate. The AUC for this blocking biosensor assay is 0.9983, with a statistical significance p-value of  $p < 0.0001$ , further supporting the high diagnostic precision and robustness of the assay.

### C. Assessment of analytical sensitivity and limit of detection

Analytical sensitivity of the blocking biosensor assay was determined by using positive and negative control serum standards from experimental cats [32]. In this evaluation, we tested serial dilutions of the serum standards, starting from a 1:4 dilution and continuing through two-fold dilutions up to 1:128, with each dilution repeated in duplicates. As presented in Figure 3A, the AuNP count per FOV for positive samples was consistently and significantly lower than that for negative controls across all tested dilutions. This reflects the inverse relationship between antibody concentration and AuNP count, where higher antibody titer serum results in greater blocking and thus fewer nanoparticles bound to the PC surface. This inverse correlation remained evident even at higher dilutions, indicating the assay's capability to distinguish between positive and negative samples over a wide dynamic range. Significant differences ( $p < 0.05$ ) were observed up to 1:128 dilution. Figure 3B demonstrated that the PI values derived from the nanoparticle counts. The dotted line represents the cut-off value at 0.5877, determined from the ROC curve analysis. The PI value for positive samples were significantly higher than those for negative samples across lower dilutions, gradually decreasing with increased dilution. The 1:8 dilution was identified as the highest dilution at which a statistically significant difference between the positive and negative groups was maintained based on PI value analysis.

### D. Blocking biosensor assay repeatability assessment

Repeatability in an assay refers to its ability to consistency in producing similar results when the same sample is prepared, processed, and measured multiple times. High repeatability is critical for ensuring the reliability and robustness of a diagnostic assay, especially when intended for translational or clinical applications. The repeatability of the blocking biosensor assay was evaluated in three conditions: (1) within the same PC, (2) between different PCs within the same assay run, and (3) across independent assay runs. All tests were conducted using a single batch of positive control serum standard. To quantify the repeatability, the coefficient of variation percentage (%CV) was calculated, as summarized in Table 1. The results showed that the %CV within a single PC was 2.04% (mean PI value of  $0.7073 \pm 0.0144$ ), indicating excellent intra-sample repeatability. The %CV between different PC within the same run was 2.71% (mean PI value of  $0.7302 \pm 0.0198$ ), suggesting minimal variability across different PC biosensor fabricated and used under identical conditions. The %CV between different runs was 4.87% (mean PI value of  $0.7150 \pm$

0.0348), reflecting good consistency when the assay was performed on different days or slightly varied environmental factors. These %CV values, all below 5%, indicate that the blocking biosensor assay is highly repeatable in diagnostic assays. These results demonstrated that the blocking biosensor assay is highly reproducible and capable of delivering consistent performance across repeated measurements, different biosensors, and independent runs.

### E. Cross-species evaluation of the blocking biosensor assay

To evaluate the cross-species assay performance of our blocking biosensor assay, we applied this assay to test serum samples collected from ferrets and deer infected with SARS-CoV-2 D614G variant, along with their respective negative controls. The antibody status of these samples had been previously confirmed through validated reference methods [32, 35, 36]. At 14 DPI, all four infected ferrets (F45, F46, F47 and F48) exhibited PI values above the established cut-off value of 0.5877, indicating a positive anti-N antibody status, while all three negative control ferrets (F25, F27 and F28) remained below cutoff value, confirming a negative antibody status, as shown in Figure 4A. Similarly, as demonstrated in Figure 4B, the assay was applied to test deer samples at 21 DPI. All four infected deer (D33, D65, D80 and D88) displayed PI values above the cut-off and were interpreted as positive for anti-N antibodies, while all three negative control deer (D34, D67 and D84) remained below the cut-off and were determined as negative.

### F. Determine timeline of seroconversion in cats infected by SARS-CoV-2

We further applied our blocking biosensor assay to monitor the antibody response dynamics in experimental cats infected with either the SARS-CoV-2 Omicron variant or D614G variant over the time course of infection. Serum samples were collected at multiple timepoints post-infection to access the timeline of seroconversion [32]. As illustrated in Figure 5, cats infected with either variant exhibited low PI values that remained below the cut-off at early time points (0, 3, and 5 DPI), comparable to uninfected control animals. By 7 DPI, a distinct increase in PI values was observed in the Omicron variant infected group, with average PI values above the cut-off threshold, while D614G variant remained below the threshold. By 14 DPI, animals infected with both Omicron and D614G variants showed robust antibody responses, with PI values well above the established cut-off. Meanwhile, the control group remained consistently negative throughout the study period. These results demonstrate that the blocking

biosensor assay is capable of detecting SARS-CoV-2 anti-N antibodies in infected cats as early as 7 DPI for Omicron variant, and 14 DPI for D614G variants.

#### IV. DISCUSSION

In this study, we developed a novel blocking biosensor assay for the detection of host antibody response induced by SARS-CoV-2. This is the first report of adapting the bELISA format into a biosensor technology platform. Compared to conventional ELISA, which typically requires several hours to complete, this biosensor assay significantly shortens the total assay time to 1 hour and 15 minutes. This enhanced performance is attributed to the digital counting of antibody-antigen complex, each labeled with an AuNP tag, providing a direct and efficient readout of antibody molecules from test samples. This substantial improvement in assay turnaround time offers a distinct advantage for rapid diagnostic applications.

In addition to the shorter testing time, the assay can reach diagnostic sensitivity and specificity of 97.80% and 98.67%, which ensured accurate discrimination between positive and negative samples. Besides the diagnostic sensitivity and specificity assessment, repeatability of the assay was evaluated, resulting in sufficient lower coefficient of variation (less than 5%) across different trials, demonstrating the assay's consistency, reliability and potential for practical use in clinical and field settings.

In our previous study [31], we identified that the mAb 127-3 specifically recognizes a conserved epitope on SARS-CoV-2 N protein and does not cross-react with the N proteins of other human or animal coronaviruses. On the other hand, since the blocking biosensor assay relies on AuNP as tags, no species-specific secondary antibody is needed, making our assay applicable across different animal species and humans.

In this study, we demonstrated that the blocking biosensor assay is capable of detecting host antibody response against SARS-CoV-2 infection in multiple animal species, including cats, ferrets, and deer.

Using the blocking biosensor assay, we are able to study the dynamics of antibody response in experimental cats infected by different SARS-CoV-2 variants. Compared with our previous study, in which serum samples were evaluated using both bELISA and serum virus neutralization assays, the earliest detectable seroconversion was observed at 14 DPI across all tested SARS-CoV-2 variants, including D614G and Omicron [31]. In the current study using the same batch of samples from infected cats, the blocking biosensor assay demonstrated improved early detection for the Omicron variant, identifying seroconversion as early as 7 DPI. For cats infected with the D614G variant, the assay was able to detect seroconversion at 14 DPI, consistent with prior

methods, but with a significantly shorter assay time. Together, these results suggest that the blocking biosensor assay enhances both the speed and earliness of antibody detection compared to previously validated methods, providing a more efficient and sensitive tool for monitoring SARS-CoV-2 infection dynamics, and enables comparison of immune response kinetics across different variants in longitudinal studies.

Compared to SARS-CoV-2 spike (S) protein, another commonly used antigen for antibody tests, the N protein offers advantages in cross-variant detection due to its higher degree of conservation across different viral strains [37, 38], which makes this N-antigen based biosensor assay more suitable for detecting the exposure from different viral variants, addressing a critical need as new viral strains continue to emerge. Additionally, since most current SARS-CoV-2 vaccines are based on the S protein rather than the N protein, our assay also have the potential to distinguish naturally infected animals from vaccinated animals. Although we did not directly evaluate this application in the present study, the use of an N protein-based detection system could be valuable for future surveillance and epidemiological studies, especially for uncovering the infection/vaccination history of SARS-CoV-2 in household and wild animals.

In conclusion, the blocking biosensor assay provides a powerful diagnostic tool with high sensitivity, specificity, and versatility necessary for managing the challenges posed by SARS-CoV-2 across various animal species. It not only enhances our diagnostic capability against current viral strains but also equips us to detect emerging variants of the virus, which is important for maintaining public health security and controlling the pandemic impact on both human and animal health.

#### V. ACKNOWLEDGEMENT

This project was supported by the National Institute of Health (Grant #R01AI166791, to YF and DD) and research funds from University of Illinois at Urbana-Champaign (to BTC). The funders had no role in study design, data collection, and analysis, decision to publish, or preparation of the manuscript. BTC discloses financial interest in Atzeyo Biosensors, a company he co-founded to commercialize the PRAM technology and assay methods.

## VI. FIGURES and LEGEND

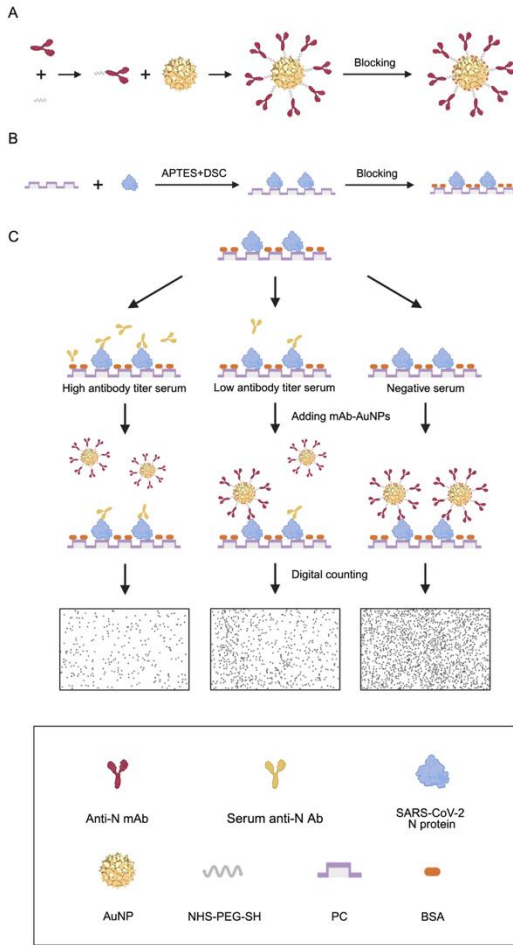


**Figure 1. Schematic illustration of blocking biosensor immunoassay for detection of host antibodies against SARS-CoV-2.** (A) Preparation of mAb-AuNPs. Anti-N mAbs were conjugated to 110 nm diameter AuNPs via SH-PEG-NHS linkers. (B) PCs were functionalized with APTES and DSC, then coated with SARS-CoV-2 N protein. Unreacted binding sites on both the AuNPs and PC surface were blocked with bovine serum albumin to reduce nonspecific interactions. (C) Serum sample was added to a PC surface coated with N protein, allowing anti-N antibodies in the serum to selectively bind to the immobilized protein. After removal of the serum, mAb-AuNPs were then introduced to react with any remaining N protein. PRAM image peak intensity values varied with the concentration of AuNPs-mAb on the PC surface. Higher anti-N antibody titers in the serum reduced the binding of mAb-AuNPs to the PC surface, reducing the AuNP count, while in negative or low-antibody titer serum, most N protein binding sites remain unoccupied, allowing extensive binding of mAb-conjugated AuNPs, which results in a higher nanoparticle count detected by PRAM microscopy.

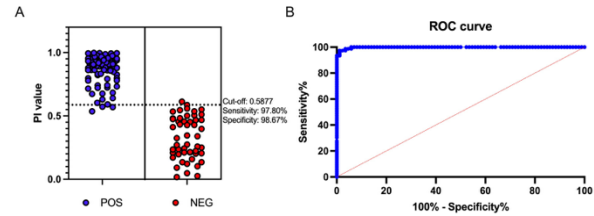


**Figure 2. Evaluation of diagnostic sensitivity and specificity of the blocking biosensor assay.** Determination of diagnostic sensitivity and specificity was conducted by testing 162 serum samples with known anti-SARS-CoV-2 antibody status (86 positives and 76 negatives). (A) A dot plot showing the distribution of the serum samples. A cut-off value of 0.5877 was selected to maximize diagnostic sensitivity and specificity. (B) A ROC curve was generated to evaluate the performance of the assay. The AUC was 0.9983 with a statistical significance of  $p < 0.00001$ . ROC analysis was carried out using GraphPad Prism.

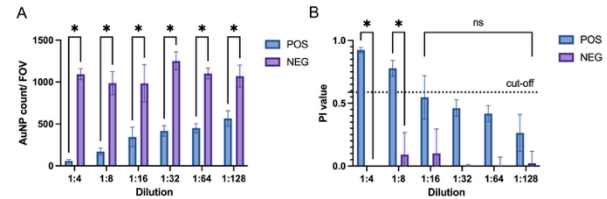


**Figure 3. Analytical sensitivity of the blocking biosensor assay in standard cat serum samples.** Two-fold serial dilutions of the high-positive and negative control serum were tested in the blocking biosensor assay to evaluate the assay's ability to detect antibodies at varying concentrations. Each data point represents the mean value of two repeats, and the error bar indicates standard deviation. (A) AuNP count per FOV for positive and negative serum standards across all tested dilutions. (B) Corresponding PI values of the results generated in panel A. The dotted line represents the previously established PI cut-off value of 0.5877. \*Statistically significant differences ( $p < 0.05$ ) between positive and negative samples. ns, no significant statistical difference.

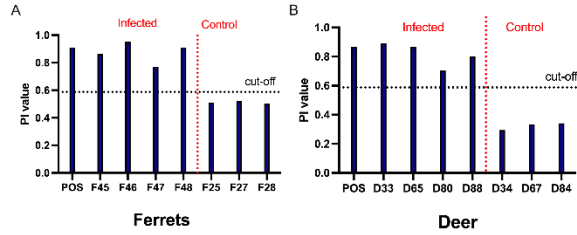


**Figure 4. Cross-species application of the blocking biosensor assay for anti-SARS-CoV-2 antibody detection in ferrets and deer.** (A) Serum samples from ferrets tested at 14 DPI; (B) Serum samples from deer tested at 21 DPI. Both animal species were infected with SARS-CoV-2 variant D614G. Dotted line represents the PI cut-off value of 0.5877. A pooled standard cat serum sample, included as a positive control (pos) in both panels.

**Table 1. Repeatability assessment of blocking biosensor assay.**

Blocking Biosensor Assay	Mean PI value	Standard deviation	%CV
Within PC	0.7073	0.0144	2.04
Between PCs	0.7302	0.0198	2.71
Between runs	0.7150	0.0348	4.87

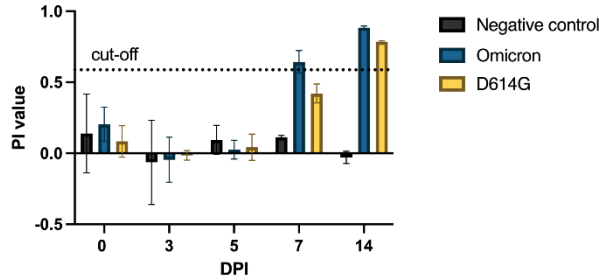


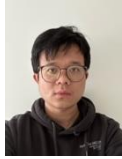
**Figure 5. Dynamics of antibody response in cats infected with SARS-CoV-2.** Serum samples were collected from two cats infected with SARS-CoV-2 variants Omicron and D614G at 0, 3, 5, 7, and 14 DPI, while samples from one negative control cat were used for comparison. The calculated PI values were plotted over time to assess the timeline of seroconversion. The dotted line represents the PI cut-off value of the block biosensor assay.

## VII. REFERENCE

- [1] P. Zhou *et al.*, "A pneumonia outbreak associated with a new coronavirus of probable bat origin," *Nature*, vol. 579, no. 7798, pp. 270-273, Mar 2020, doi: 10.1038/s41586-020-2012-7.
- [2] M. A. A. Mahdy, W. Younis, and Z. Ewaida, "An Overview of SARS-CoV-2 and Animal Infection," *Front Vet Sci*, vol. 7, p. 596391, 2020, doi: 10.3389/fvets.2020.596391.
- [3] J. C. Rotondo *et al.*, "SARS-CoV-2 Infection: New Molecular, Phylogenetic, and Pathogenetic Insights. Efficacy of Current Vaccines and the Potential Risk of Variants," *Viruses*, vol. 13, no. 9, Aug 25 2021, doi: 10.3390/v13091687.
- [4] H. Lee *et al.*, "Rapid detection of intact SARS-CoV-2 using designer DNA Nets and a pocket-size smartphone-linked fluorimeter," *Biosens Bioelectron*, vol. 229, p. 115228, Jun 1 2023, doi: 10.1016/j.bios.2023.115228.
- [5] B. D. Kevadiya *et al.*, "Diagnostics for SARS-CoV-2 infections," *Nat Mater*, vol. 20, no. 5, pp. 593-605, May 2021, doi: 10.1038/s41563-020-00906-z.
- [6] A. M. Jankelow *et al.*, "Smartphone clip-on instrument and microfluidic processor for rapid sample-to-answer detection of Zika virus in whole blood using spatial RT-LAMP," *Analyst*, vol. 147, no. 17, pp. 3838-3853, Aug 22 2022, doi: 10.1039/d2an00438k.
- [7] J. Lim *et al.*, "Microfluidic point-of-care device for detection of early strains and B.1.1.7 variant of SARS-CoV-2 virus," *Lab Chip*, vol. 22, no. 7, pp. 1297-1309, Mar 29 2022, doi: 10.1039/d2lc00021k.
- [8] B. Zhao, C. Che, W. Wang, N. Li, and B. T. Cunningham, "Single-step, wash-free digital immunoassay for rapid quantitative analysis of serological antibody against SARS-CoV-2 by photonic resonator absorption microscopy," *Talanta*, vol. 225, p. 122004, 2021.
- [9] D. M. Rissin *et al.*, "Single-molecule enzyme-linked immunosorbent assay detects serum proteins at subfemtomolar concentrations," *Nature biotechnology*, vol. 28, no. 6, pp. 595-599, 2010.
- [10] N. H. Ferrin *et al.*, "Validation of a blocking enzyme-linked immunosorbent assay for detection of antibodies against porcine reproductive and respiratory syndrome virus," *Clin Diagn Lab Immunol*, vol. 11, no. 3, pp. 503-14, May 2004, doi: 10.1128/CDLI.11.3.503-514.2004.
- [11] M. Drobysh *et al.*, "Biosensors for the Determination of SARS-CoV-2 Virus and Diagnosis of COVID-19 Infection," *Int J Mol Sci*, vol. 23, no. 2, Jan 8 2022, doi: 10.3390/ijms23020666.
- [12] A. Yakoh, U. Pimpitak, S. Rengpipat, N. Hirankarn, O. Chailapakul, and S. Chaiyo, "Paper-based electrochemical biosensor for diagnosing COVID-19: Detection of SARS-CoV-2 antibodies and antigen," *Biosens Bioelectron*, vol. 176, p. 112912, Mar 15 2021, doi: 10.1016/j.bios.2020.112912.
- [13] S. K. Elledge *et al.*, "Engineering luminescent biosensors for point-of-care SARS-CoV-2 antibody detection," *Nat Biotechnol*, vol. 39, no. 8, pp. 928-935, Aug 2021, doi: 10.1038/s41587-021-00878-8.
- [14] Y. Zhao *et al.*, "Rapid, Multispecies Detection of SARS-CoV-2 Antibodies via a Meta-Surface Plasmon Resonance Biosensor," *Transbound Emerg Dis*, vol. 2024, p. 9350822, 2024, doi: 10.1155/2024/9350822.
- [15] H. I. Peng and B. L. Miller, "Recent advancements in optical DNA biosensors: exploiting the plasmonic effects of metal nanoparticles," *Analyst*,

- vol. 136, no. 3, pp. 436-47, Feb 7 2011, doi: 10.1039/c0an00636j.
- [16] B. Cunningham, B. Lin, J. Qiu, P. Li, J. Pepper, and B. Hugh, "A plastic colorimetric resonant optical biosensor for multiparallel detection of label-free biochemical interactions," *Sensors and Actuators B: Chemical*, vol. 85, no. 3, pp. 219-226, 2002.
- [17] B. T. Cunningham *et al.*, "Label-free assays on the BIND system," *SLAS Discovery*, vol. 9, no. 6, pp. 481-490, 2004.
- [18] B. Cunningham, P. Li, B. Lin, and J. Pepper, "Colorimetric resonant reflection as a direct biochemical assay technique," *Sensors and Actuators B: Chemical*, vol. 81, no. 2-3, pp. 316-328, 2002.
- [19] C. J. Choi and B. T. Cunningham, "A 96-well microplate incorporating a replica molded microfluidic network integrated with photonic crystal biosensors for high throughput kinetic biomolecular interaction analysis," *Lab Chip*, vol. 7, no. 5, pp. 550-6, May 2007, doi: 10.1039/b618584c.
- [20] W. Liu, S. Li, E. Chow, S. Bhaskar, Y. Fang, and B. T. Cunningham, "Photonic Crystal Enhanced Microscopy on a 2D Photonic Crystal Surface," *Advanced Materials Technologies*, vol. 10, no. 6, 2025, doi: 10.1002/admt.202401837.
- [21] T. D. Canady *et al.*, "Digital-resolution detection of microRNA with single-base selectivity by photonic resonator absorption microscopy," *Proc Natl Acad Sci U S A*, vol. 116, no. 39, pp. 19362-19367, Sep 24 2019, doi: 10.1073/pnas.1904770116.
- [22] C. Che *et al.*, "Activate capture and digital counting (AC + DC) assay for protein biomarker detection integrated with a self-powered microfluidic cartridge," *Lab Chip*, vol. 19, no. 23, pp. 3943-3953, Dec 7 2019, doi: 10.1039/c9lc00728h.
- [23] Y. Zhuo *et al.*, "Single nanoparticle detection using photonic crystal enhanced microscopy," *Analyst*, vol. 139, no. 5, pp. 1007-15, Mar 7 2014, doi: 10.1039/c3an02295a.
- [24] C. Che *et al.*, "Accelerated Digital Biodetection Using Magneto-plasmonic Nanoparticle-Coupled Photonic Resonator Absorption Microscopy," *ACS Nano*, vol. 16, no. 2, pp. 2345-2354, Feb 22 2022, doi: 10.1021/acsnano.1c08569.
- [25] S. Ghosh *et al.*, "A compact photonic resonator absorption microscope for point of care digital resolution nucleic acid molecular diagnostics," *Biomed Opt Express*, vol. 12, no. 8, pp. 4637-4650, Aug 1 2021, doi: 10.1364/BOE.427475.
- [26] B. Zhao *et al.*, "Digital-resolution and highly sensitive detection of multiple exosomal small RNAs by DNA toehold probe-based photonic resonator absorption microscopy," *Talanta*, vol. 241, p. 123256, May 1 2022, doi: 10.1016/j.talanta.2022.123256.
- [27] Bhaskar S *et al.*, "Chapter 6 - Nano-engineering at functional photonic crystal interfaces," in *Nano-Engineering at Functional Interfaces for Multi-Disciplinary Applications*, S. B. Sai Sathish Ramamurthy, Narendra Reddy Ed., 2025, pp. 123-156.
- [28] Y. Xiong *et al.*, "Microscopies Enabled by Photonic Metamaterials," *Sensors (Basel)*, vol. 22, no. 3, Jan 30 2022, doi: 10.3390/s22031086.
- [29] H. Lee *et al.*, "Physically grounded deep learning-enabled gold nanoparticle localization and quantification in photonic resonator absorption microscopy for digital resolution molecular diagnostics," *Biosens*

- Bioelectron*, vol. 281, p. 117455, Aug 1 2025, doi: 10.1016/j.bios.2025.117455.
- [30] K. Khemtonglang *et al.*, "Portable, smartphone-linked, and miniaturized photonic resonator absorption microscope (PRAM Mini) for point-of-care diagnostics," *Biomed Opt Express*, vol. 15, no. 10, pp. 5691-5705, Oct 1 2024, doi: 10.1364/BOE.531388.
- [31] F. Yuan *et al.*, "Development of monoclonal antibody-based blocking ELISA for detecting SARS-CoV-2 exposure in animals," *mSphere*, vol. 8, no. 4, p. e0006723, Aug 24 2023, doi: 10.1128/msphere.00067-23.
- [32] M. Martins *et al.*, "The Omicron variant BA. 1.1 presents a lower pathogenicity than B. 1 D614G and Delta variants in a feline model of SARS-CoV-2 infection," *Journal of virology*, vol. 96, no. 17, pp. e00961-22, 2022.
- [33] C. Chen *et al.*, "Spatial and temporal clustering of anti-SARS-CoV-2 antibodies in Illinois household cats, 2021-2023," *PLoS One*, vol. 19, no. 5, p. e0299388, 2024, doi: 10.1371/journal.pone.0299388.
- [34] W. Liu *et al.*, "Dynamic and large field of view photonic resonator absorption microscopy for ultrasensitive digital resolution detection of nucleic acid and protein biomarkers," *Biosens Bioelectron*, vol. 264, p. 116643, Nov 15 2024, doi: 10.1016/j.bios.2024.116643.
- [35] M. Martins *et al.*, "From Deer-to-Deer: SARS-CoV-2 is efficiently transmitted and presents broad tissue tropism and replication sites in white-tailed deer," *PLoS Pathog*, vol. 18, no. 3, p. e1010197, Mar 2022, doi: 10.1371/journal.ppat.1010197.
- [36] M. V. Palmer *et al.*, "Susceptibility of white-tailed deer (*Odocoileus virginianus*) to SARS-CoV-2," *J Virol*, vol. 95, no. 11, May 10 2021, doi: 10.1128/JVI.00083-21.
- [37] A. Royster *et al.*, "SARS-CoV-2 Nucleocapsid Protein Is a Potential Therapeutic Target for Anticoronavirus Drug Discovery," (in eng), *Microbiol Spectr*, vol. 11, no. 3, p. e0118623, Jun 15 2023, doi: 10.1128/spectrum.01186-23.
- [38] J. Cubuk *et al.*, "The SARS-CoV-2 nucleocapsid protein is dynamic, disordered, and phase separates with RNA," *Nature communications*, vol. 12, no. 1, pp. 1-17, 2021.



**Siyan Li** received the Master's degree in Pathobiology from the University of Illinois at Urbana-Champaign in 2024. He is interested in apply bioengineering technology for animal diseases diagnostics.



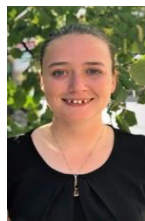
**Weijing Wang** received her Ph.D. and M.Eng. degrees in Bioengineering from the University of Illinois Urbana-Champaign and her B.S. in Clinical Laboratory Medicine from Hubei University of Chinese Medicine. Her research expertise lies in biosensing diagnostics, with a strong background in assay development, bioconjugation, and nanofabrication. She has contributed significantly to the development of cutting-edge detection platforms integrating photonic nanomaterials, CRISPR-Cas, and microfluidic chips for ultrasensitive immunoassays, as well as nucleic acid and intact virus detection.



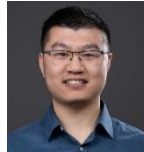
**Weinan Liu** is an Electrical Engineering PhD candidate at the University of Illinois Urbana-Champaign (UIUC). He received his M.S. in Physics from the Sun Yat-Sen University (SYSU). He has published more than 10 international peer-reviewed journals and conference proceedings. He is a recipient of Mavis Future Faculty Fellowship. His research focused on metaphotonic devices, plasmonics, and microscopic imaging for biomedical applications.



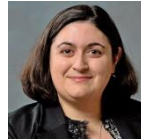
**Chi Chen** received the Bachelor's degree in Veterinary Medicine in 2020 from Nanjing Agricultural University, Nanjing, China. He is pursuing the Ph.D. degree in pathobiology from University of Illinois at Urbana-Champaign. His is interested in epidemiology, diagnostic assay development for animal infectious disease control.



**Skye Shepherd** is a pursuing a Ph.D. in Bioengineering from the University of Illinois at Urbana-Champaign, and has a Bachelor's degree in Biomedical Engineering from Boston University. She has been developing non-enzymatic methods using toehold-mediated strand displacement for ultrasensitive nucleic acid and protein detection. Her research focuses on optical biosensors using digital detection and surface functionalization.



**Fangfeng Yuan** received his PhD degree in Pathobiology from University of Illinois at Urbana-Champaign in 2022. He is currently a postdoctoral fellow at Massachusetts Institute of Technology. His research interests lie in novel delivery platforms for vaccine development and lentiviral engineering for broad applications.



**Jennifer Reihhart** received her DVM from the University of Illinois in 2010. Following a rotating internship at Cornell University, she completed her residency in Small Animal Internal Medicine at Kansas State University and was boarded in 2014. She received her PhD in comparative biomedical sciences from the University of Wisconsin in 2017 and obtained board-certification in the American College of Veterinary Clinical Pharmacologists in 2019. Since 2017, Dr. Reinhart has served as an Assistant Professor of Small Animal Internal Medicine at University of Illinois.



**Diego Diel** is an Associate Professor at Department of Population Medicine and Diagnostic Sciences, College of Veterinary Medicine, Cornell University, Ithaca, NY. Dr. Diel's research focuses the molecular mechanisms underlying virus-host interactions and more specifically on the mechanisms underlying viral immune evasion that contribute to virus virulence and disease pathogenesis.



**Brian T. Cunningham** is a professor of Electrical and Computer Engineering, Bioengineering, and Chemistry at the University of Illinois at Urbana-Champaign. He is a Fellow of IEEE, NAI, AAAS, AIMBE, RSC, and Optica. Prof. Cunningham's research interests include nanophotonics, electromagnetics, optics, micro/nanofabrication, biosensors, microfluidics. Application areas that he pursues include point of care cancer molecular diagnostics, infectious disease diagnostics, environmental monitoring, and development of new tools for life science research.



**Ying Fang** is a Professor at the Department of Pathobiology, Carl R. Woese Institute for Genomic Biology, University of Illinois at Urbana-Champaign. She is a Fellow of National Academy of Inventors. Prof. Fang's research interests have been focused on understanding the basic molecular mechanism of viral pathogenesis and apply the basic knowledge to develop vaccines and diagnostic assays.